J|A|C|S
ARTICLES
Published on Web 06/22/2004

Sequential Arrangement of γ-Valerolactone Enantiomers Enclathrated in Cholic Acid Channels as Studied by ^{13}C Solid-State NMR: Elucidation of the Optical Resolution Mechanism

Shinji Nakamura, F. Imashiro, K. Takegoshi,* and Takehiko Terao

Contribution from the Department of Chemistry, Graduate School of Science, Kyoto University, Kyoto 606-8502, Japan

Received January 30, 2004; E-mail: takeyan@kuchem.kyoto-u.ac.jp

Abstract: The mechanism of the optical resolution of γ-valerolactone (VAL) enantiomers by enclathration in cholic acid (CA) channels was investigated. ^{13}C cross-polarization magic-angle spinning spectra of CA/VAL inclusion compounds show four methyl ^{13}C peaks of VAL with different intensities depending on the enantiomeric ratios. The four peaks were assigned to the inner and end (*S*)-(−)-enantiomers (**S**) in the **S** domain and the inner and end (*R*)-(+)-enantiomers (**R**). The relative intensities of the four methyl ^{13}C peaks cannot be explained by the random process model for inclusion but are successfully reproduced by assuming the first-order Markov process, in which the inclusion probabilities of **S** and **R** depend on which enantiomer has precedingly entered the CA channel. The probability $p_{S/S}$ that two **S** enantiomers successively enter a channel is thus found to be 83%, and $p_{R/R}$ is 50%. The large probability of $p_{S/S}$ indicates that once an **S** enantiomer enters a channel, it become easy for other **S** enantiomers to successively enter the channel, and thus the large enantiomeric excess of **S** is obtained. The inclusion probabilities of **S** and **R** were confirmed by 1D $^{13}C-^{13}C$ polarization-transfer experiments among the four methyl carbons of VAL in the CA channel. Further, we found that the ^{13}C line widths and peak positions of the CA tail group change depending on the enantiomeric ratio. We concluded that once **S** is included, it changes the conformation of the CA tail group so that other **S** enantiomers become easy to successively enter the channel.

Introduction

Inclusion compounds have attracted much attention in both basic chemistry and practical applications. Only guest molecules with size and stereo structure fit to the cavity formed by host molecules are selectively trapped in the cavity. Molecular recognition is a fundamental phenomenon in both chemistry and biology. From this point of view, it is interesting and important to investigate how to discriminate guest molecules at the inclusion into the host cavities in the inclusion compounds.

Cholic acid (CA; see Chart 1) is a host compound exhibiting efficient optical resolution of racemic lactones not only by recrystallization from liquid lactones but also by absorption into the channels in the CA crystal.[1] The CA/γ-valerolactone (VAL) 1:1 inclusion compound (CA/VAL) from racemic VAL includes (*S*)-(−)-VAL enantiomer (abbreviated hereafter as **S**) and (*R*)-(+)-VAL enantiomer (**R**) with the **S**/**R** ratio of ca. 2:1.[1] The molecular structures of **S** and **R** are schematically shown in Chart 1. An X-ray crystal structure analysis of CA/VAL showed that CA molecules form channels, and the CA channel has deep side pockets (cavity) formed by the tail parts of CA molecules with a VAL molecule per cavity.[2,3] The conformations of VAL

Chart 1. Cholic Acid (CA) and **S** and **R** Enantiomers of γ-Valerolactone

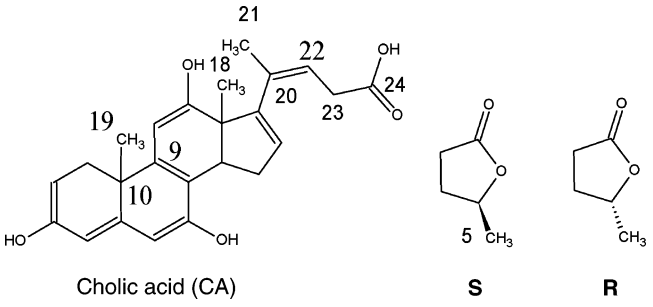

enantiomers in the CA channel were determined by comparing the ^{13}C chemical-shift tensor principal values measured using one-dimensional switching-angle spinning solid-state NMR and those calculated using the ab initio GIAO method:[4] **S** has the methyl group in the equatorial position to the five-membered ring of VAL, while **R** has it in the axial direction.

In this study, we determine statistics governing the VAL enantiomer arrangement in the CA channel of CA/VAL formed by the absorption method and examine the change of the CA

(1) Miyate, M.; Shibakami, M.; Takemoto, K. *J. Chem. Soc., Commun.* **1988**, 655−656.
(2) Miyata, M.; Shibakami, M.; Chirachanchai, S.; Takemoto, K.; Kasai, N.; Miki, K. *Nature* **1990**, *343*, 446−447.
(3) Miki, K.; Kasai, N.; Shibakami, M.; Takemoto, K.; Miyata, M. *J. Chem. Soc., Chem. Commun.* **1991**, 1757−1759.
(4) Imashiro, F.; Kuwahara, D.; Terao, T. *J. Chem. Soc., Perkin Trans.* **1993**, *2*, 1759−1763.

10.1021/ja049463l CCC: $27.50

tail part depending on the enantiomeric ratio using ^{13}C solid-state NMR. On the basis of these results, we discuss the mechanism of the optical resolution of VAL enantiomers by the inclusion into the CA channels.

Experimental Section

Samples. Commercially available CA was recrystallized from methanol and dried under vacuum at 100 °C for 24 h. Four kinds of VAL were prepared as follows: Labeled racemic [5-$^{13}C^2H_3$] VAL (^{13}C,^2H ~99%) was synthesized in the same way as previously described.[4] Nonlabeled racemic VAL was purchased from Nacalai Tesque. Nonlabeled **S**-rich VAL was prepared by repeating absorption and distillation of VAL five times, whereas nonlabeled **R**-rich VAL was obtained by filtering VAL remaining after inclusion of racemic VAL into the CA channel. The **S/R** enantiomeric ratios of **S**-rich VAL and **R**-rich VAL were 95:5 and 37:63, respectively, which were determined by ^1H solution-state NMR using the chiral shift reagent (*R*)-(−)-2,2,2-trifluoro-1-(9-anthryl)ethanol.

CA/VAL was obtained by pouring each VAL on solid CA. A ^{13}C,^2H-labeled sample CA/[5-$^{13}C^2H_3$] VAL (CV-L) was prepared from racemic [5-$^{13}C^2H_3$] VAL with the molar ratio of VAL/CA = 3. Three nonlabeled samples of CA/**S**-rich VAL (CV-A), CA/racemic VAL (CV-B), and CA/**R**-rich VAL (CV-C) were prepared from **S**-rich VAL, racemic VAL, and R-rich VAL, respectively, with VAL/CA = 2. After each mixture was kept at ca. −10 °C for 48 h or over, crystallites were collected and washed with hexane and propyl ether to remove excess VAL.

NMR Experiments. The solid-state NMR experiments were carried out using a Chemagnetics CMX-400 spectrometer operating at the resonance frequency of 100.66 MHz for ^{13}C. A cross-polarization (CP)/magic-angle spinning (MAS) probe (Doty Sci. Inc) with a 5 mm rotor system was used. The rf field strengths for high-power proton decoupling and CP were 80 kHz and 55 kHz, respectively. The contact time for CP was 2.5 ms, and the recycling time was 20 s. The MAS frequency was kept constant within ±10 Hz by a control system. For the ^{13}C observation in CV-L, ^2H double-quantum (DQ) decoupling[5] was applied in addition to ^1H decoupling with the ^2H rf field strength of 30 kHz. One-dimensional (1D) $^{13}C-^{13}C$ polarization-transfer experiments were performed for CV-L by using the pulse sequence shown in Figure 1, in which the initial ^{13}C polarization is selectively prepared with a chemical-shift-filter pulse sequence named SELDOM.[6]

Results and Discussion

Peak Assignments of the Methyl Carbons of VAL in CA/VAL. Figure 2 shows a ^{13}C MAS spectrum of CV-L (CA/[5-$^{13}C^2H_3$]VAL) which was measured using a single ^{13}C $\pi/2$ pulse under ^1H and ^2H decoupling. The recycling time was 60 s, which is about 10 times as long as the longitudinal relaxation times T_{1C} of 5−7 s, so that the observed spectrum is quantitative. Four methyl carbon peaks are observed at 20.1, 20.4, 21.0, and 21.3 ppm, which we refer to as SI, SB, RB, and RI, respectively; the reason of the naming will become clear below. The relative intensities for these four peaks were obtained by fitting the observed line shape to a sum of four Lorentz functions, which are listed in Table 1. The spectrum of nonlabeled CV-B (Figure 3b) shifts to the high-frequency side by 0.8 ppm compared to that of CV-L: the chemical shifts of SI, SB, RB, and RI are 20.9, 21.2, 21.8, and 22.1 ppm, respectively. The observed shifts between the two spectra can be ascribed to deuteration effects of the methyl protons on the ^{13}C chemical shift. Such deuteration effects are frequently observed in solution-state ^{13}C NMR and are attributed to the difference of bond distances between $^{13}C-^1H$ and $^{13}C-^2H$.[7] In the previous ^{13}C CP/MAS spectrum of a nonlabeled sample,[4] only two peaks were observed at 21.1 and 22.0 ppm for **S** and **R**, respectively, probably because apodization by a fast decay function deteriorated the spectral resolution

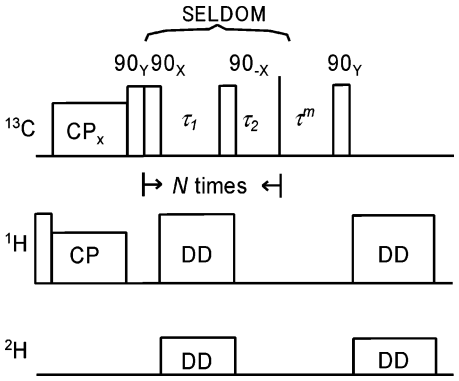

Figure 1. Pulse sequence for the 1D $^{13}C-^{13}C$ polarization-transfer experiment. The transverse ^{13}C magnetization created by CP is nonselectively converted to the longitudinal magnetization by the first $\pi/2$ pulse. The initial polarization gradient is prepared by selectively exciting a VAL methyl ^{13}C peak with the SELDOM sequence [$90_X-\tau_1-90_{-X}-\tau_2$] repeated for *N* times. SELDOM starts with a $\pi/2$ pulse followed by a τ_1 period during which CW decoupling is applied for both ^1H and ^2H. This permits the transverse ^{13}C magnetization to evolve solely under the effect of the isotropic chemical shift. The second $\pi/2$ pulse converts the *Y* component of the transverse magnetization to the longitudinal magnetization, while the *X* component is left unaffected. In the τ_2 period, the remaining transverse magnetization decays by T_2. The longitudinal magnetization is used as the initial magnetization for polarization transfer during the mixing time τ^m.

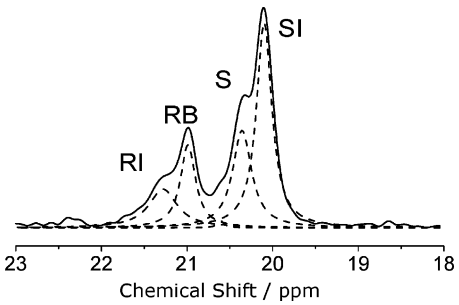

Figure 2. ^{13}C MAS spectrum of a CA/VAL inclusion compound CV-L under ^1H and ^2H decoupling and MAS with a spinning frequency of 4.5 kHz. The ^{13}C peaks were fitted to four Lorentzian line-shape functions (broken lines). The four peaks were assigned to the ^{13}C-labeled methyl carbons (SI, SB, RR, and RI; see Chart 2) of the VAL molecules in the CA channel.

Table 1. Observed Methyl ^{13}C Intensities and Calculated Populations for the VAL Molecules in the Four CA/VAL Samples

		loading condition	experimental				calculated[b]			
	m_s[a]	VAL/CA	SI	SB	RB	RI	SI	SB	RB	RI
CV-A	0.95	2.0	100	0	0	0	96	3	1	0
CV-B	0.50	2.0	45	21	18	16	41	25	22	12
CV-C	0.37	2.0	24	24	24	28	24	26	26	24
CV-L	0.50	3.0	45	25	20	10	45	25	21	9

[a] Initial mole fraction of **S** in the liquid VAL, which was determined by solution-state ^1H NMR using the chiral shift reagent. [b] Calculated assuming the first-order Markov process for inclusion of VAL enantiomers into the CA channel.

(5) (a) Pines, A.; Ruben, D. J.; Vega, S.; Mehring, M. *Phys. Rev. Lett.* **1976**, *36*, 110−113. (b) Pines, A.; Vega, S.; Mehring, M. *Phys. Rev. B* **1978**, *18*, 112−125.
(6) Tekely, P.; Brondeau, J.; Elbayed, K.; Retounard, A.; Canet, D. *J. Magn. Reson.* **1988**, *80*, 509−516.
(7) Berger, S. *Carbon-13 studies of deuterium labeled compounds: Encyclopedia of Nuclear Magnetic Resonance*; Wiley: New York, 1996.

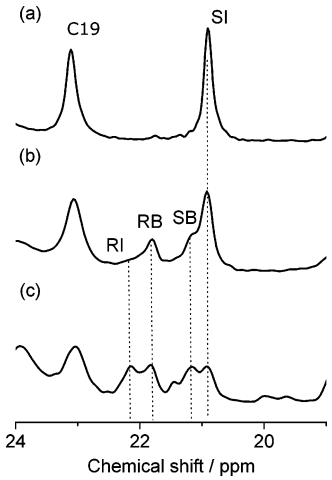

Figure 3. ^{13}C CP/MAS spectra of CA/VAL inclusion compounds obtained with different loading conditions: (a) CV-A, (b) CV-B, and (c) CV-C. The peak at 23.0 ppm is assigned to C19 of CA. The vertical lines at 20.9, 21.2, 21.2, and 21.8 ppm show the peak positions of the SI, SB, RB, and RI methyl carbons of the VAL molecules, respectively. The peak intensities of the methyl carbons and the loading conditions are listed in Table 1.

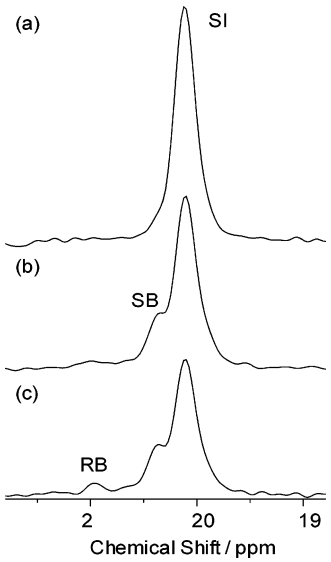

Figure 4. 1D ^{13}C polarization-transfer spectra of CV-L acquired by using the pulse sequence in Figure 1 under the MAS frequency 1.0 kHz. The carrier frequency for the SELDOM sequence was set on resonance to the SI peak. To improve the selectivity of the SI peak, we combined two SELDOM sequences with different τ_1 values: one SELDOM sequence ($N = 1$) with $\tau_1 = 9.2$ ms for removal of the SB peak and the second SELDOM ($N = 8$) with $\tau_1 = 2.8$ ms for removal of the RI and RB peaks. The τ_2 period is 1 ms. The SELDOM sequence is followed by a mixing period of 0 s (a), 0.30 s (b), and 0.75 s (c).

and because the magnetic field was lower (4.7 T) than that in the present experiment (9.4 T). Closely examining the previous spectrum, however, we can recognize that each peak has a shoulder peak on the high frequency side, and the spectrum is essentially the same as the present one.

Figure 3 shows three ^{13}C CP/MAS spectra of CV-A, CV-B, and CV-C, which were prepared from nonlabeled VAL with **S/R** enantiomeric ratios of 95:5, 50:50, and 37:63, respectively. The intensities of the four methyl peaks (SI, SB, RB, and RI) in the three samples are also collated in Table 1. For CV-A, in which no appreciable amount of **R** is included, only the SI peak is observed at 20.9 ppm (Figure 3a). Therefore, we can assign the SI peak to the methyl carbon of **S**. Figure 4 shows the mixing-time dependence of the spectrum of labeled sample CV-L observed by the 1D polarization-transfer experiment which starts with the initial magnetization of SI by using the pulse sequence in Figure 1 with the MAS frequency of 1.0 kHz. The initial spectrum ($\tau^m = 0$) in Figure 4a shows a good selectivity achieved by SELDOM. At $\tau^m = 0.3$ s, the intensity of SI decreases, while the SB peak appears (Figure 4b). In general, the cross-peak is ascribed to polarization transfer processes such as chemical exchange or conformational interconversion. We also performed the same exchange experiment but at a higher MAS frequency of 4.5 kHz and found that the SB peaks disappears. At such a higher MAS frequency, dynamic process being unaffected, the weak ^{13}C−^{13}C dipolar couplings between VAL methyl carbons are removed, so that the cross-peak due to polarization transfer should disappear. Therefore, its disappearance of the SB peak at the spinning frequency of 4.5 kHz indicates that the exchange mechanism is due to polarization transfer. Hence, the appearance of the SB peak at the short mixing time (Figure 4b) shows that SB is located most closely to SI. At $\tau^m = 0.75$ s, the SB peak intensity increases further, and at the same time, the RB peak appears (Figure 4c). From this result, the RB carbon proves to be located one more further than the SB carbon from the SI carbon adjacent to the latter. Here, we assume that the **S** and **R** methyl carbons facing each other at the boundary between the **S** and **R** domains have chemical shifts different from the inner **S** and **R** methyl carbons,

Chart 2. Schematic Illustration of a Domain Structure in the VAL Enantiomer Arrangement

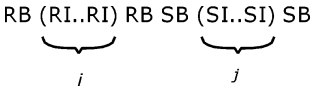

respectively, owing to the **S**−**R** enantiomer interaction. Then, we can assign the peaks of SI, SB, RB, and RI on the basis of the above observations: the SI peak can be assigned to the inner **S** methyl carbons because CV-A, which includes almost only **S**, shows only the SI peak; we use the same symbols for distinction of different methyl carbons as those of different peaks. The result of the 1D exchange NMR probes that the SB and RB signals are ascribed to the boundary **S** (SB) and boundary **R** (RB) carbons, respectively. The RI signal, which does not appear even for the mixing time of 0.75 s (Figure 4c), is due to the inner **R** carbons (RI), which are the farthest from the SI carbons. We schematically illustrate the domain structure of **S** and **R** in Chart 2.

Statistics of the VAL Enantiomer Arrangement. In this section, we examine statistics governing the VAL enantiomer arrangement in the CA channel, simulating the observed intensities profile of the VAL methyl ^{13}C signals on the basis of the Bernoulli process and the Markov process. Application of the Markov process in host/guest systems can also be found in describing crystal growth of a polar inclusion compound of racemic perhydrotriphenylene with 1-(4-nitrophenyl)piperazine as a guest molecule.[8]

First, we treat the case where the quantity of liquid VAL is infinite. A conceivable absorption process is the Bernoulli process,[9] in which **S** or **R** enters the CA channel independently of the enantiomers already entered, with the constant probability

(8) König, O.; Bürgi, H.-B.; Armbruster, T.; Hulliger, J.; Weber, T. *J. Am. Chem. Soc.* **1997**, *119*, 10632−10640.

P(S) or P(R), respectively (P(S) + P(R) = 1). In this case, P(S) coincides with the enantiomeric fraction f_S of **S** in the CA channel. f_S can be measured by ^{1}H NMR of a solution of VAL using a chiral shift reagent or ^{13}C CP/MAS NMR of powdered CA/VAL. Using the probability p_A that enantiomer **A** in an infinite quantity of racemic VAL enters the CA channel, we can represent P(A) for general VAL as

$$P(A) = \frac{m_A p_A}{m_S p_S + m_R p_R} \quad (1)$$

where m_A is the mole fraction of enantiomer **A** in liquid VAL.

Another possible inclusion process is the Markov process,[9−11] where the probability of **S** or **R** entering a CA channel depends on the VAL enantiomer arrangement in the CA channel. Here, we discuss only the first-order Markov process: the inclusion probability of **S** or **R** depends only on which enantiomer has precedingly entered the CA channel. We can describe the first-order Markov process using the four conditional probabilities $p_{A/B}$ (**A**, **B** = **S** or **R**) that **B** in racemic VAL enters the CA channel immediately after **A**. Owing to the conservation relations of $p_{S/S} + p_{S/R} = 1$ and $p_{R/S} + p_{R/R} = 1$, only two of the four are independent; we use $p_{S/S}$ and $p_{R/R}$ to describe the first-order Markov process, hereafter. The probability P_A(B) that **B** enters the CA channel following **A**, in general VAL, is given by

$$P_A(B) = \frac{m_B p_{A/B}}{m_S p_{A/S} + m_R p_{A/R}} \quad (2)$$

The enantiomeric fraction f_S is equal to the sum of the two probabilities of the **S**−**S** connection and the **R**−**S** connection:

$$f_S = f_S P_S(S) + (1 - f_S) P_R(S) \quad (3)$$

Using eqs 2 and 3, we can calculate P_A(B) for various $p_{S/S}$ (or $p_{R/R}$) if m_S and f_S are given.

In the above two cases, we assumed the quantity of VAL to be infinite, so that m_A is constant. Actually, however, the VAL/CA molecular ratio is finite, and therefore m_S decreases due to optical resolution by CA as the inclusion process advances. In this case, it would hardly be possible to analytically calculate the relative ^{13}C peak intensities. Hence, we numerically obtained VAL enantiomer arrangement. To do so, we scaled down a prepared system of CA and liquid VAL to a small system composed of 10^3 CA molecules forming a single channel and VAL enantiomers with the actual molecular number ratio of CA, **S**, and **R**. Then, we simulated a VAL enantiomer arrangement by repeating the inclusion of **S** or **R** enantiomer according to the probability of eq 1 for the random process and eq 2 for the first-order Markov process, taking into account the change of m_S with the progress of inclusion. We repeated this procedure a thousand times and confirmed that the fluctuations of calculated enantiomer fractions and triplet populations fall within 0.1%. In a real system, the channel length distributes; this distribution should affect enantiomer fractions, triplet populations, and the like. In our simulations using a Lorentzian distribution function, however, such effects are so small that we do not practically need to change the results calculated by a single channel model.

Figure 5. Calculated arrangements of VAL enantiomers in the CA host channel. The random process with $p_S = 0.74$ (a) and the first-order Markov statistics with $p_{S/S} = 0.83$ and $p_{R/R} = 0.50$ (b) were assumed for the inclusion process of VAL enantiomers. The filled and open rectangles express **S** and **R**, respectively. Each VAL arrangement is a part of the VAL arrangement calculated for a CA channel with 10^3 cavities.

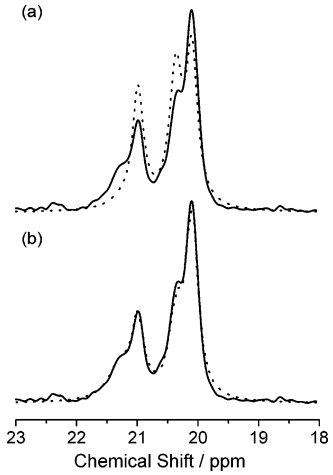

Figure 6. Experimental and simulated ^{13}C spectra of CV-L. The experimental spectra (solid line) are identical with the spectrum in Figure 2. The simulated spectra (broken line) are the sum of four Lorentzian functions with the area intensity ratios of (a) 35:35:27:3 (random process) and (b) 45:25:21:9 (first-order Markov process) for the SI, SB, RB, and RI peaks.

First, we simulate the observed VAL-$^{13}CH_3$ peak intensities in CV-L using the initial molar ratio of $m_S/m_R/m_{CA}$ = 1.5:1.5:1, assuming the random inclusion process. The observed f_S value of 70% in CV-L, which is given by the sum of the observed intensity fractions of SI and SB, gives the value of p_S to be 0.74. In Figure 5a, we show a part of the VAL enantiomer arrangement simulated using the random process model with $p_S = 0.74$. Counting the number M_A of **A** (**A** = SI, SB, RB, or RI) in the calculated VAL arrangement, we can obtain the relative intensities $I_A^{calcd} = M_A/\sum M_A$ of the four peaks to be $I_{SI}^{calcd}/I_{SB}^{calcd}/I_{RB}^{calcd}/I_{RI}^{calcd}$ = 35:35:27:3. The simulated spectrum using these intensities $I_A{}^{calcd}$ is shown in Figure 6a, indicating a serious difference from the observed spectrum. This result proves that the inclusion process does not obey the random process.

In the case of the first-order Markov process, the observed value of 70% gives the following constraint between $p_{S/S}$ and $p_{R/R}$:

$$p_{R/R} = -1.69 + 2.64 p_{S/S} \quad (4)$$

To determine the most reliable value of $p_{S/S}$, we obtain the populations I_A^{calcd} of the individual four enantiomers from VAL arrangements calculated for various $p_{S/S}$ and compared them with the populations with the peak intensities I_A^{expt}. Figure 7

(9) Hoel, P. G.; Port, S. C.; Stone, C. J. *Introduction to Stochastic Process*; Houghton Mifflin: Boston, MA, 1972.
(10) Harris, K. D. M.; Jupp, P. E. *Proc. R. Soc. London, Ser. A* **1997**, *453*, 333−352.
(11) Fredrickson, G. H.; Milner, S. T.; Leibler, L. *Macromolecules* **1992**, *25*, 6341−6354.

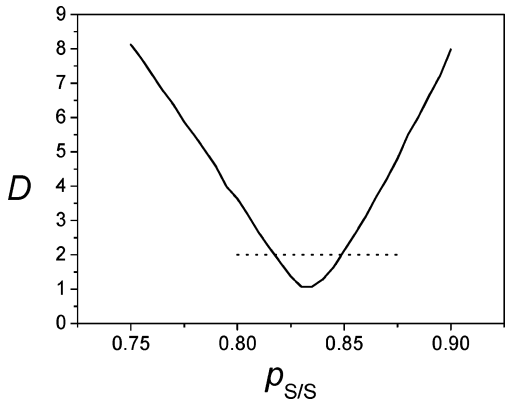

Figure 7. $p_{S/S}$ dependence of the root-mean square difference D (in %) between the experimental and calculated area intensities of the four methyl carbon peaks in CV-L. The calculation was made by assuming the first-order Markov process for inclusion of the two VAL enantiomers into CA host channels. The dotted line indicates the average difference of 2%.

shows the root-mean square difference D between I_A^{calcd} and I_A^{expt} as a function of $p_{S/S}$:

$$D(p_{S/S}) = \left[\frac{1}{4}\sum_A (I_A^{expt} - I_A^{calcd})^2\right]^{1/2} \quad (5)$$

The position of the minimum gives the best fit $p_{S/S} = 0.83$ and, therefore, $p_{R/R} = 0.50$ from eq 4. Using these values, the VAL arrangement was obtained as shown in Figure 5b. Both **S** and **R** domains are generally long in length compared to those for the random process: once an **S** enantiomer enters a CA channel, it becomes easy for other **S** enantiomers to successively enter the CA channel, making long **S** series because of $p_{S/S} > p_S$. Similarly, long **R** series also occur owing to $p_{R/R} > p_R$. The relative intensities of $I_{SI}^{calcd}/I_{SB}^{calcd}/I_{RB}^{calcd}/I_{RI}^{calcd} = 45:25:21:9$ were obtained from the calculated VAL arrangements, providing the simulated spectrum in Figure 6b; the agreement with the experimental spectrum is excellent. Using $p_{S/S} = 0.83$ and $p_{R/R} = 0.50$, we further simulated the other VAL enantiomer arrangements in CV-A, CV-B, and CV-C. The calculated populations of SI, SB, RB, and RI are collated in Table 1. These calculated values are in good agreement with the corresponding experimental ones. Thus the intensity profiles of VAL methyl carbons in all samples are well explained by a statistical model that the inclusion probability of an **S** or **R** enantiomer depends on which enantiomer has been precedingly included, being $p_{S/S} = 0.83$ and $p_{R/R} = 0.50$.

Validity of the First-Order Markov Model for the Inclusion of VAL. In this section, we examine the validity of the first-order Markov model for the inclusion of VAL enantiomers into CA channels, including the possibility of a higher-order Markov process by analyzing the $^{13}C-^{13}C$ polarization-transfer experimental results obtained for CV-L. In the short mixing-time region of the polarization-transfer experiment, polarization transfer occurs between the two methyl ^{13}C spins of the adjacent VAL molecules and the mixing-time dependence of the magnetization almost governed by the probability $P_A(B)$ that **B** enters the CA channel immediately after **A**. In the long mixing-time region, polarization transfer between the second nearest ^{13}C spins also occurs. The mixing-time dependence of the magnetization thus reflects the probability $P_{AB}(C)$ that enantiomer **C** enters the channel immediately after the **A**−**B** arrangements. Examining whether an experimental value of $P_{AB}(C)$ is given by the $P_A(B)P_B(C)$ value calculated using $p_{S/S} = 0.83$ and $p_{R/R} = 0.50$ or not, we can determine whether the Markov process is of the first-order or higher.

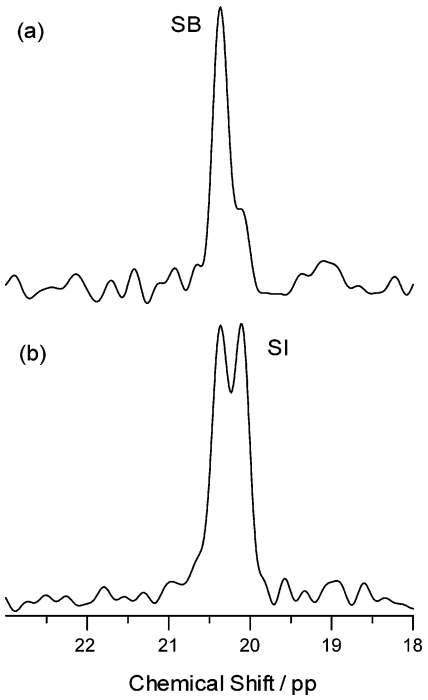

Figure 8. Boundary selective ^{13}C polarization-transfer spectra acquired by the pulse sequence of CP-π/2-SELDOM(SI)-τ_2^m-π/2-SELDOM(SB)-τ_2^m-π/2. The first SELDOM(SI) sequence is the selective excitation pulse for the SI peak, and the second SELDOM(SB) is applied to remove the SI peak, leaving the SB peak. $\tau_1^m = 0.3$ s and $\tau_2^m = 0$ s (a) and 0.3 s (b). The relative intensities of the SI and SB peaks were 13% and 87% (a) and 44% and 56% (b), respectively.

Before simulating the polarization-transfer experiments, we determine the polarization-transfer rate between the methyl ^{13}C spins of two adjacent VAL enantiomers. For this purpose, we performed a boundary-selective polarization-transfer experiment by selecting the peak of SB adjacent to SI in the $(SI)_k-SB-RB$ arrangement as the initial magnetization. The boundary selective polarization-transfer experiment was made by introducing the two mixing-time periods τ_1^m and τ_2^m and the two SELDOM periods of SELDOM(SI) and SELDOM(SB), being schematically represented as CP-π/2-SELDOM(SI)-τ_1^m-π/2-SELDOM(SB)-τ_2^m-π/2, where SELDOM(SI) and SELDOM(SB) are the selective sequences for SI and SB, respectively. The first half of the whole pulse sequence, CP-π/2-SELDOM(SI)- τ_1^m with $\tau_1^m = 0.3$ s, prepares the polarization giving the spectrum in Figure 4b, which contains the selected SI polarization and the SB polarization transferred from the SI polarization. Applying the second SELDOM(SB) sequence, we achieved the SB peak-only spectrum at $\tau_2^m = 0$ (Figure 8a); correctly, the SI peak with a relative intensity of 0.13 remains, and therefore the SB peak intensity is 0.87. After a second mixing time τ_2^m of 0.3 s, the spectrum shown in Figure 8b was observed, showing only the SI and SB peaks with almost the same amplitude. The absence of the RB peak indicates that the polarization-transfer rate for the SB−RB pair is much lower than that for the SB−SI pair. By ignoring polarization transfer between SB and RB, the polarization-transfer process can be

described by the rate equation for the three spins in the SI^1-SI^2-SB arrangement

$$\frac{d}{dt}\begin{pmatrix} m_{SI^1}(t) \\ m_{SI^2}(t) \\ m_{SB}(t) \end{pmatrix} = -\begin{pmatrix} k_1 & -k_1 & 0 \\ -k_1 & 2k_1 & -k_1 \\ 0 & -k_1 & k_1 \end{pmatrix}\begin{pmatrix} m_{SI^1}(t) \\ m_{SI^2}(t) \\ m_{SB}(t) \end{pmatrix} \quad (6)$$

where we assumed that the polarization-transfer rates for the SI^1-SI^2 pair and the SI^2-SB pair are equal to each other. We apply eq 6 to the polarization-transfer process during τ_2^m, assuming the initial polarizations to be $m_{SI^1}(0) = m_{SI^2}(0) = 0.065$ and $m_{SB}(0) = 0.87$. We calculated the intensities of the SI and SB peaks for various k_1 values. The agreement of the calculated intensities for the SI and SB peaks with the observed ones in Figure 8b is achieved with a polarization-transfer rate k_1 of 2.2 s^{-1}. This value will be used for the analysis of the polarization-transfer curves below.

For simulating the polarization-transfer curves, we consider a ^{13}C spin arrangement with the distance r_i between the ith and $i+1$th spins ($i = 1, \cdots, N-1$). We denote the polarization of the ith VAL ^{13}C spin as $p^i(t)$ ($-1 \le p^i(t) \le 1$). The time dependences of the N polarizations are described by a differential equation:

$$-\frac{d\vec{P}(t)}{dt} = \mathbf{W}\vec{P}(t) \quad (7)$$

where $\vec{P}(t)$ is the column vector with the components of $p^1(t)$, $p^2(t), \cdots, p^N(t)$, and $\mathbf{W}$ is the rate matrix representing the ^{13}C polarization transfer and the ^{13}C longitudinal relaxation. The components $W_{i,j}$ of the matrix $\mathbf{W}$ are given by

$$W_{i,i\pm1} = \begin{cases} -k_1 & \text{for } \mathbf{S}-\mathbf{S} \text{ and } \mathbf{R}-\mathbf{R} \\ -k_2 & \text{for } \mathbf{S}-\mathbf{R} \end{cases}$$

$$W_{i,i} = \frac{1}{T_1^i} - \sum_{j=i-2,i-1,i+1,i+2} W_{i,j},$$

$$W_{i,i\pm2} = \frac{-W_{i,i\pm1}W_{i\pm1,i\pm2}}{(W_{i,i\pm1}^{1/6} + W_{i\pm1,i\pm2}^{1/6})^6}$$

and

$$W_{i,j} = 0 \text{ for } j \neq i, i \pm 1, i \pm 2 \quad (8)$$

where k_1 denotes the rate of the ^1H-driven polarization transfer between two adjacent enantiomers of the same kind ($\mathbf{S}-\mathbf{S}$ and $\mathbf{R}-\mathbf{R}$), k_2 represents the rate for the adjacent $\mathbf{S}-\mathbf{R}$ pair, and T_1^i is the longitudinal relaxation time of the ith ^{13}C spin. We use the value (2.2 s^{-1}) obtained from the boundary selective polarization-transfer experiment for k_1 and treat k_2 as an adjustable parameter. To determine T_1^i, we measured ^{13}C longitudinal magnetization decays at the high MAS frequency limit under which k_1 and k_2 become zero. At the MAS frequency of 4.3 kHz, we observed four single-exponential decays with the time constants of $(T_1^{SI}, T_1^{SB}, T_1^{RB}, T_1^{RI}) = (5.7, 4.3, 6.7, 5.6)$/s for the four VAL-methyl ^{13}C peaks. The single exponential decays with different T_1 indicate that the effect of the $^{13}C-^{13}C$ polarization transfer is negligibly small.

To solve the polarization-transfer behavior, we express $\vec{P}(t)$ for a short interval $\Delta t (\ll 1/k_1, 1/k_2, 1/T_1)$ by a linear relation:

$$\vec{P}(t + \Delta t) = [1 - \Delta t\mathbf{W}]\vec{P}(t) \equiv \mathbf{Q}\vec{P}(t) \quad (9)$$

We obtain $\vec{P}(t)$ by progressively expanding it as

$$\vec{P}(t) = \mathbf{Q}\vec{P}(t - \Delta t) = \mathbf{Q}^2\vec{P}(t - 2\Delta t) = \cdots = \mathbf{Q}^n\vec{P}(0) \quad (10)$$

The resulting individual polarizations ($i = 1-N$) in a given arrangement are summed up for each SI, SB, RB, and RI to give their peak intensities.

We performed polarization-transfer experiments for four different initial ^{13}C polarizations of SI, SB, RB, and RI; the results are shown in Figure 9. We calculated the $p_{S/S}$ and k_2 dependence of the root-mean-square deviation (rmsd) between the experimental and calculated polarization-transfer curves. The minimum of rmsd was found for $p_{S/S} = 0.83$ and $k_2 = 0.23$ s^{-1}; the polarization-transfer curves simulated using these values are also shown in Figure 9. The value $p_{S/S} = 0.83$ is the same as deduced by analyzing the peak intensities (Figure 7).

The error of a best-fit $p_{S/S}$ of 0.83 is estimated by calculating $F(p_{S/S})$ defined as[14]

$$F(p_{S/S}) = \frac{\xi^2(p_{S/S}) - \xi^2(0.83)}{\xi^2(0.83)}(N - M) \quad (11)$$

where N denotes the number of the experimental data, M is the number of adjustable parameters, and $\xi^2(p_{S/S})$ represents the rmsd at $p_{S/S}$ for $k_2 = 0.23$ s^{-1}. The function $F(p_{S/S})$ statistically obeys the F distribution of the freedom $(1, N - M)$, and the value of $F(p_{S/S})$ is expected to be less than 7 for the 99% confidence. The $F(p_{S/S})$ function is shown in Figure 10 with the 99% confidence line. From this result, we obtained $p_{S/S} = 0.83 \pm 0.01$ and also $p_{R/R} = 0.50 \pm 0.02$ from eq 4, for the 99% confidence.

Next, we examine the possibility that the inclusion process obeys the Markov process of the second-order rather than the first-order. The second-order Markov process is represented by the four probabilities of $p_{S/S/S}$, $p_{S/R/S}$, $p_{R/S/S}$, and $p_{R/R/S}$ that an **S** enantiomer enters the CA channel immediately after the **S**−**S**, **S**−**R**, **R**−**S**, and **R**−**R** arrangements, respectively. For the first-order Markov process, the probabilities turn $p_{R/S/S} = p_{S/S/S} = p_{S/S} = 0.83$ and $p_{S/R/S} = p_{R/R/S} = p_{R/S} = 0.50$. We determined the values of $p_{S/S/S}$, $p_{S/R/S}$, $p_{R/S/S}$, and $p_{R/R/S}$ reproducing the experimental data of the four methyl peak intensities and the polarization-transfer curves and found $p_{S/S/S} = 0.83 \pm 0.02$, $p_{S/R/S} = 0.54 \pm 0.10$, $p_{R/S/S} = 0.86 \pm 0.10$, and $p_{R/R/S} = 0.50 \pm 0.03$. The larger error for $p_{R/S/S}$ and $p_{S/R/S}$ indicates that the dependence of the polarization-transfer curves on these probabilities is lower. This is probably attributed to the smaller value of k_2 than k_1. The best fit probabilities obtained for the second-order Markov model are almost in agreement with the values expected from the first-order Markov model. Hence, we may conclude that the inclusion process in CA/VAL is governed by the first-order Markov process with $p_{S/S} = 0.83$ and $p_{R/R} = 0.50$.

(12) Meier, B. H. *Polarization transfer and SD in solid-state NMR: Adv. Mag. Opt. Res.*; Academic Press: London, 1994.
(13) Kubo, A.; McDowell, C. A. *J. Chem. Soc., Faraday Trans.* **1988**, *84*, 3713−3730.
(14) Bevington, P. R.; Robinson, D. R. *Data reduction and error analysis for physical science*, 2nd ed.; McGraw-Hill: New York, 1992.

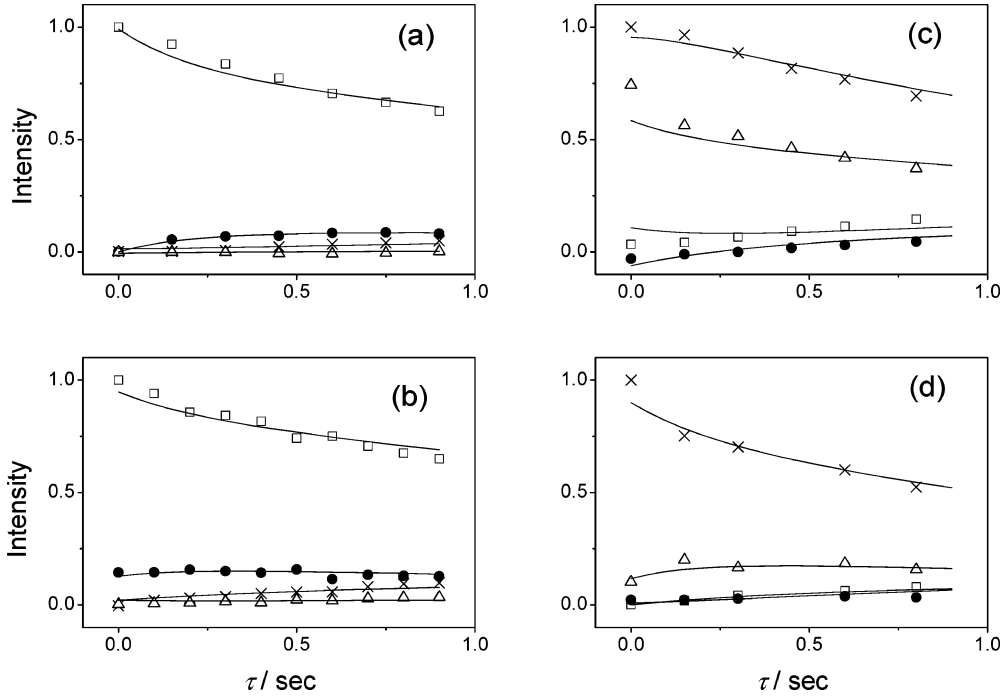

Figure 9. Mixing-time dependence of the ^{13}C magnetization in the 1D polarization-transfer experiments with the MAS frequency of 1.0 kHz. The symbols □, ●, ×, and △ denote SI, SB, RB, and RI, respectively. The initial ^{13}C polarizations for SI, SB, RB, and RI are [1, 0, 0, 0] (a), [1, 0.3, 0, 0] (b), [0, 0, 1, 0.8] (c), and [0, 0, 1, 0.1] (d), respectively. The curves are the best-fitted curves obtained by applying eq 7.

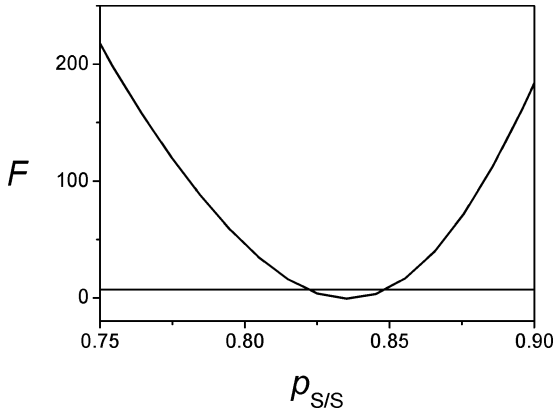

Figure 10. $F(p_{S/S})$ between the four experimental and simulated polarization-transfer curves in Figure 9. The dotted line describes the region of the 99% confidence between the experimental and the simulated ones.

We consider the difference of the two polarization-transfer rates of 2.2 s^{-1} and 0.23 s^{-1} which were obtained from the above experiments. The shift difference σ among the VAL methyl carbons is much smaller than the $^{13}C-^{1}H$ dipolar broadening, being unable to cause the difference of the two rates. The difference of k_1 and k_2 can be attributed to the difference of the $^{13}C-^{13}C$ distances between homo- and heteroenantiomers. It is known that VAL molecules undergo quasi-isotropic overall reorientation with the rate of a few tens of Hz in the CA channel,[4] which is higher than the polarization-transfer rates. We assume that the $^{13}C-^{13}C$ distance between VAL methyl groups can be replaced by the center-to-center distance r of the VAL enantiomers: the polarization-transfer rate k is proportional to r^{-6}.[12,13] Here, we assume that a rate k_1 of 2.2 s^{-1} for adjacent homoenantiomers corresponds to the center-to-center distance of 0.44 nm for the two adjacent VAL molecules, which was determined by X-ray diffraction studies.[2,3] Then, from the value $k_2 = 0.23$ s^{-1}, the center-to-center distance between adjacent

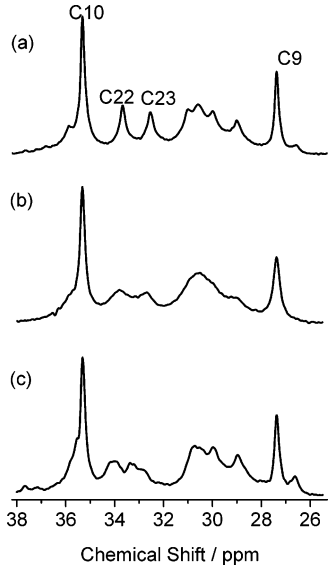

Figure 11. ^{13}C CP/MAS spectra of CV-A (a), CV-B (b), and CV-C (c) in the range of 25.5−38.0 ppm.

SB−RB enantiomers is estimated to be 0.64 nm, which is substantially longer than that between adjacent homoenantiomers. This fact may indicate that stereo interference is stronger between heteroenantiomers than between homoenantiomers.

Optical Resolution Mechanism of CA/VAL. Figure 11 shows ^{13}C CP/MAS spectra of CV-A (a), CV-B (b), and CV-C (c). The overlapped line shape around 32−34 ppm differs among the three spectra. The two peaks at 32.4 and 33.5 ppm in Figure 11a are due to the C23 and C22 carbons of the tail part of CA in CV-A, respectively. These peaks significantly shift to the high-frequency side and broaden in CV-B and CV-C. Such shifts were also observed for the other tail carbons C20, C21, and C24 and broadening for C19, C20, and C21. On the other hand,

no appreciable shift nor broadening was observed for the skeleton carbons of CA except for the C19 carbon peak. These facts suggest that the conformation of the tail part in CA is altered by inclusion of the VAL enantiomer, depending on whether the adjacent enantiomer is **S** or **R**, therefore, a distribution of the conformation results, causing such line shifts and broadening.

When the fact that the CA tail parts form the CA channel is considered, the above results present the following inclusion mechanism of CA/VAL: When an **S** enantiomer enters a CA channel, it deforms the tail part of each CA molecule existing from the entrance of the CA channel to the depth of the entered **S** enantiomer, so that it becomes easy for other **S** enantiomers to successively enter the CA channel ($p_{S/S} = 0.83$). However, once an **R** enantiomer happens to be included, the tail parts of CA in the passage deform in such a way to exhibit a neutral preference for either enantiomer ($p_{R/S} = p_{R/R} = 0.50$). Thus, there exist two states of the channel: one favors the inclusion of **S** (state 1), and the other shows no preference (state 2). When the channel state is state 2 (1), the inclusion of an **S** (**R**) enantiomer switches the state to state 1 (2), while the inclusion of an **R** (**S**) enantiomer does not change it.

Previously we indicated that the included **S** enantiomer has the methyl group in the equatorial position to the five-membered ring and **R** has it in the axial position and further that the energy difference between the two conformers in the liquid state practically explains the observed **S**/**R** enantiomeric ratio in the CA channel.[4] Therefore, it was suggested that the optical resolution by inclusion is caused by the energy difference in the conformations of VAL. If this is the case, however, the inclusion process should result in the random arrangement of **S** and **R** depicted in Figure 4a. Our present study has proved that the inclusion of VAL enantiomers into the CA channel obeys the Markov process, denying the above optical resolution mechanism. However, the deformation of the CA channel in response to the inclusion of **S** enantiomers would be such that not only **S** enantiomers are preferred to **R** enantiomers but also equatorial **S** (axial **R**) enantiomers enter much more easily than axial **S** (equatorial **R**) enantiomers. The larger population of the equatorial conformation in liquid VAL may be a cause of the high value of $p_{S/S}$, together with the deformation of the CA tail parts which drives successive inclusion of **S** enantiomers.

Acknowledgment. This research was supported by a Grant-in-Aid for Science Research from the Ministry of Education, Culture, Sports, Science, and Technology.

JA049463L